Durable antimicrobial adhesion cotton textiles based on borneol-based anti-MRSA finishing agent

Jiangqi Xu (xujiangqi@btbu.edu.cn)
Beijing Technology and Business University
Xia Li
Beijing Technology and Business University
Wenjing Yu
Beijing Technology and Business University
Xing Wang
Beijing University of Chemical Technology
Jianzhong Ma
Shaanxi University of Science and Technology

Research Article

Keywords: Cotton textiles, Anti-superbug, Borneol, One-step finishing, Stereochemical antimicrobial adhesion

Posted Date: October 25th, 2021

DOI: https://doi.org/10.21203/rs.3.rs-1001756/v1

Durable antimicrobial adhesion cotton textiles based on borneol-based anti-MRSA finishing agent

Jiangqi Xu[a, *], Xia Li[a], Wenjing Yu[a], Xing Wang[b], Jianzhong Ma[c]

[a] School of Light Industry, Beijing Technology and Business University, Beijing 100048, P. R. China

[b] Beijing Laboratory of Biomedical Materials, Beijing University of Chemical Technology, Beijing 100029, P. R. China

[c] College of Bioresources Chemical and Materials Engineering, Shaanxi University of Science and Technology, Xi'an 710021, Shaanxi, P. R. China

* Corresponding author. Dr. Jiangqi Xu; E-mail address: xujiangqi@btbu.edu.cn

Abstract

There is an urgent need to develop novel antimicrobial cotton textiles (CT) because microbial contamination is one of the greatest threats to public health due to the emerging of infectious diseases and drug-resistant pathogens. In this work, an isocyanate group containing borneol-based antimicrobial finishing agent (NCO-B) was developed which can be covalently grafted to the surface of cotton textiles by a simple one-step method. The obtained NCO-B-finished CT (NCO-B-CT) exhibited broad-spectrum antimicrobial adhesion properties against bacteria (*E. coli*), including superbugs (MRSA), and fungi (*A. niger*). Due to its unique antimicrobial mechanism of borneol stereochemistry, the obtained NCO-B-CT is a non-releasing antimicrobial material which causes no skin sensitization and has no cytotoxicity. The mechanical properties of the CT were also improved after this finishing process. Additionally, it displayed durable washing fastness and antimicrobial properties by bearing 50

times laundering cycles. Therefore, this material may have great potential for application in multifunctional textiles, flexible skin electronics and medical protection.

Graphic abstract

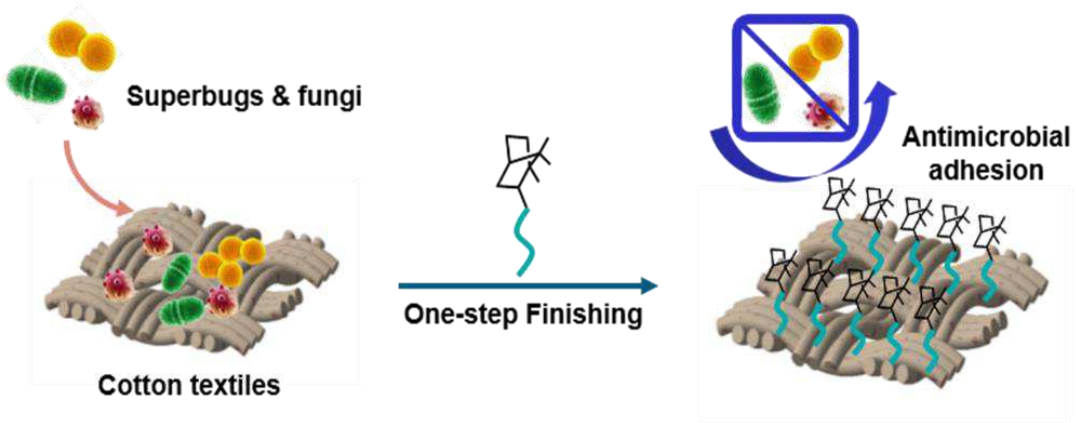

Keywords: Cotton textiles; Anti-superbug; Borneol; One-step finishing; Stereochemical antimicrobial adhesion

1. Introduction

Public health emergency driven by emerging infectious diseases is at the forefront of global awareness (Metcalf et al. 2017). Cotton textiles (CT), which are widely used in hospitals, hotels and other public environments, can easily become sources of infection and cause pathogenic organism transmission (Bains et al. 2019; Cao et al. 2020; Lin et al. 2014; Munoz-Price et al. 2012). Even worse, antibiotics abuse has created an unprecedented environment for the evolution of superbugs, which are extremely dangerous and difficult to treat, posing an increasing threat to public health (Brown et al. 2016; Qian et al. 2018; Velema et al. 2013; Wang et al. 2017b; Yu et al. 2016). Thus, there is an urgent need to develop novel and effective antimicrobial CT materials and reduce the use of antibiotics (Yang et al. 2020).

Substantial efforts have been made to develop antimicrobial CT using various kinds antimicrobials compounds, such as metal and oxide nanoparticles (El-Naggar et al. 2021; Su et al. 2021; Thi and Lee 2017), nanocomposite particles (Errokh et al. 2021; Irfan et al. 2019), hybrid particles (Gao et al. 2021a; Karimi et al. 2014), chitosan and cationic compounds (Gao et al. 2020; Gu et al. 2018; Sadeghi-Kiakhani et al. 2018), *N*-halamines (Pan et al. 2018; Wang et al. 2018) and guanidine (Cai et al. 2018; Li et al. 2018), etc. Generally, the antimicrobial activity of CT can be achieved by physical incorporating of antimicrobial compounds during extrusion or chemical immobilizing of them on the surface of fabrics (Gao et al. 2021b; Ye et al. 2021). Thus, the CT antimicrobial modes can be categorized into release killing (Simoncic et al. 2010; Wu et al. 2016) and contact killing (Duan et al. 2020). For release killing mode, the durability of antimicrobial performances cannot be guaranteed and the release of antimicrobial agents potentially cause the microbes resistance (Yang et al. 2020; Ye et al. 2021; Zhang et al. 2016). In addition, the gradually leaching of biocide will contaminate the

environment (Zhang et al. 2016) and impact the wearer's skin resident flora (Hoefer et al. 2011; Xin et al. 2020), which is originally beneficial to skin health as they can resist the growth of pathogenic bacteria (Bouslimani et al. 2015; Gu et al. 2018; Simoncic et al. 2010). Alternatively, contact-killing strategy can kill the bacteria on the CT surfaces, but the antibacterial ability may be gradually diminished after a period of use, as the live/dead bacteria could adhere on the fabrics to form biofilm that is difficult to be removed (Lin et al. 2018).

Recently, the emerging bacterially antiadhesive or antifouling strategy by employing functional groups with special wettability (Qian et al. 2017) such as zwitterions (Chen et al. 2011; Chen et al. 2016; Zhang et al. 2018), polyhydroxy (Wang et al. 2017a) and fluoride (Lin et al. 2018; Song et al. 2019) may offer a solution for the safe and durable use of antimicrobial CT. Meanwhile, because superbugs primarily stem from antibiotic misuse, the strategy of antimicrobial adhesion is believed to be a superior choice for the development of antimicrobial CT, which can prevent bacteria from evolving into superbugs, as well as resist the adhesion and further proliferation or contamination of superbugs. As an alternative, a new surface stereochemistry strategy for antimicrobial adhesion was proposed (Li et al. 2017; Li et al. 2021; Luo et al. 2014; Shi et al. 2015; Sun et al. 2016; Xin et al. 2020; Xu et al. 2018; Xu et al. 2019a), which can control the microbial adhesion behavior by utilizing the "chiral taste" of microbes (Wang et al. 2010; Wang et al. 2012; Xie et al. 2020). In this strategy, surface stereochemistry plays a significant role in regulating microbial behavior during the interaction between microorganisms and material surfaces, rather than hydrophobicity or the release of bactericides (Lin et al. 2017). It is therefore considered to be a soft management and control of microbes, rather than kill them (Xu et al. 2019a). Our previous studies demonstrated that chiral borneol based polymers that can control microbial adhesion due to their "chiral taste" (Luo et al. 2014),

and this property is also suitable for CT decoration.

Borneol decorated antimicrobial CT (BDCT) has been developed through a two-step method using siloxane as linker, which exhibited antimicrobial adhesion properties owing to the influence of the surface bicyclic-stereochemistry of borneol, rather than hydrophobicity (Xu et al. 2019a). However, the siloxane tends to self-condensate during the first modification and the two-step finishing process is not efficient. In addition, the anti-superbug performance of borneol-modified CT has not been researched. In this study, a facile and cost-effective strategy through direct covalent grafting of an isocyanate group (NCO)-containing borneol-based antimicrobial finishing agent (NCO-B) without any additional linker was investigated. As shown in Scheme 1, the NCO group of NCO-B can react easily with the OH group of CT under mild conditions. The obtained NCO-B-finished CT (NCO-B-CT) presented broad-spectrum and perdurable antimicrobial adhesion properties against common bacteria (*E. coli*), superbugs (MRSA) and fungi (*A. niger*). Additionally, the safety (i.e. skin sensitization, cytotoxicity), washing durability and mechanical properties of NCO-B-CT were also confirmed.

2. Experimental section

2.1. Materials

CT (40 × 40 s bleached twill cotton fabric, weighing 185 g/m^2) was purchased from a local fabric store. L-Borneol (97%) was purchased from Sigma-Aldrich. Isophorone diisocyanate (IPDI, 99%), dibutyltin dilaurate (DBTDL, 98%), tetrahydrofuran (THF, AR) and N,N-dimethylformamide (DMF, AR) were purchased from J&K Scientific. 3-(4,5-dimethylazolyl-2)-2,5-diphenyltetrazolium bromide (MTT) was purchased from Tokyo Chemical Industry (TCI). Malt extract agar, tryptone soy agar (TSA) and trypticase soy broth (TSB) were purchased from Aladdin. The BacLight live/dead kit

(Molecular Probes) was purchased from Thermo Fisher Scientific. Other reagents were purchased from Sinopharm Chemical Reagent Co., Ltd, China. *Escherichia coli* (*E. coli*, ATCC 25922), methicillin-resistant *Staphylococcus aureus* (MRSA, ATCC 43300), *Aspergillus niger* (*A. niger*, CICC 41254) were obtained from the China Center of Industrial Culture Collection. Mouse fibroblast cells (L929) were obtained from Cell Resource Center, IBMS, CAMS/PUMC, Beijing, China. Roswell Park Memorial Institute (RPMI) 1640 medium, fetal bovine serum (FBS), penicillin and streptomycin were purchased from Gibco BRL, Gaithersberg, MD, USA.

2.2. Synthesis of NCO-B

The NCO-borneol (NCO-B) was synthesized by the reaction between isocyanate (NCO) group of isophorone diisocyanate and OH group of borneol (Scheme 1) (Chen et al. 2016; Fujimori et al. 2015). Briefly, 2.05 g of L-borneol (13.3 mmol) and 3.53 g of IPDI (15.9 mmol) were dissolved in 20 mL of dry THF, followed by the addition of DBTDL (0.1 mL) under a nitrogen atmosphere. The reaction mixture was stirred at 50 °C for 12 h. The product was obtained as a white solid after repeated dissolution in THF and precipitation in petroleum ether for three times. Upon drying, the NCO-B was obtained in a yield of 90%.

2.3. Preparation of NCO-B-CT

The NCO group of NCO-B can easily react with the OH group of CT (Scheme 1) (Chen et al. 2016). The finishing process was as follows. The CT was firstly treated by ultrasonically washing with dimethylacetamide, acetone, and water in sequence for 10 min before they were dried at 90 °C for 5 min. The overall process was repeated three times and the clean CT were obtained for further use. Thereafter, the clean CT was immersed in 5 wt% NCO-B/DMF finishing agent (liquor ratio 20:1) for 10 min. Then the textiles were baked for 1 h at 80 °C, dried for 2 min at 130 °C. Finally, the NCO-B-

CT can be obtained after washing thoroughly with deionized water and drying.

2.4. Characterization and measurement

Structures of NCO-B was characterized by FTIR spectroscopy (IR Affinity-1, SHIMADZU) and ^{1}H NMR (JNM-ECA400, JEOL). The surface morphologies of CT and NCO-B-CT were observed by scanning electron microscopy (SEM, JSM-7800F, JEOL, Tokyo, Japan). Energy-dispersive spectrometry (EDS, Hitachi S-4700, Tokyo, Japan), attenuated total reflection Fourier transform infrared spectroscopy (ATR-FTIR, Perkin-Elmer Spectrum 100 spectrometer, Waltham, MA, USA) and X-ray photoelectron spectroscopy (XPS, Thermo Fisher Scientific, Waltham, MA, USA) were used to analyze the surface chemical composition and structure of CT before and after finishing. Water contact angle (WCA) measurement was performed at room temperature on a JC2000D3 (Zhongyi Kexin Technology Co., Ltd., Beijing, China) to study the wettability of raw CT and NCO-B-CT. The whiteness of the textiles was detected by an SC-80C automatic chronometer (Kang Guang Instrument Co., Ltd., Beijing, China) and it was calculated under D65 illumination and CIE 1964 standard observer (Jafari et al. 2007); each sample was measured at three different positions, with each reported value representing the means of five samples. The degree of grafting (DG) of NCO-B-CT was investigated by gravimetric method and calculated as follows (Yu et al. 2016):

$$DG\ (\%) = (W_g - W_0) / W_0 \times 100 \quad (1)$$

where W_0 is the weight of raw CT and W_g is the weight of NCO-B-CT.

2.5. Antibacterial adhesion assessment

Antibacterial adhesion tests were carried out based on a modified GB/T 20944.3-2008 method and ASTM E2149 method by using gram-negative bacterium (*E. coli*) and gram-positive superbug (MRSA) (Song et al. 2019; Wang et al. 2017a). Before antibacterial adhesion tests, the strains were cultivated in

fresh TSB medium at 37 °C with a shaking incubator overnight. The bacterial suspension was then diluted to a concentration of 10^7 CFU mL^{-1} by sterile normal saline for later use.

Antibacterial Adhesion Rate of NCO-B-CT. The sample treatment before testing was performed according to the following procedure: first, raw CT and NCO-B-CT were incubated with 3 mL of bacterial suspension (10^7 CFU mL^{-1}) at 37 °C for 4 h. After rinsing with sterile normal saline three times to remove the unadhered bacteria, the bacteria strongly adhered to the surface of the samples were dispersed into 3 mL of sterile normal saline via an ultrasonic cleaner. After that, taken out 100 μL of dispersion and serially diluted with sterile normal saline. Finally, a 100 μL diluted bacterial solution was coated on TSA medium and further cultured for 24 h at 37 °C. The colonies of the bacteria on the agar plate were counted and the number of adhered bacteria was calculated by multiplying the number of colonies by the dilution factor. Each experiment was carried out three times and the significant differences of CT and NCO-B-CT for each bacteria type were obtained by statistical analysis. In addition, calculate the $\log_{10}$ reduction in bacterial adhesion count of NCO-B-CT. The data were presented as mean ± standard deviation (SD). The antibacterial adhesion rate of NCO-B-CT as compared to raw CT was calculated using the following equation (Chen et al. 2016):

$$\text{Antibacterial adhesion rate (\%)} = (A - B) / A \times 100 \quad (2)$$

where A and B are the colony-forming units (CFUs) of raw CT and NCO-B-CT, respectively.

Morphology of Bacterial Adhesion on the Treated Fabrics. Bacterial adhesion on the treated fabrics was intuitively observed by SEM (S-4700 Hitachi) after the adhesion experiments. The samples mentioned above were immobilized through 2.5% glutaraldehyde for 2 h at 4 °C. Then, the fixed bacteria were dehydrated by gradient ethanol (50, 60, 70, 80, 90, and 100%), respectively. Finally, the samples were vacuum-dried for 12 h prior to the SEM observation.

Live/Dead BacLight Bacterial Viability Assay for Bacterial Adhesion on the Treated Fabrics. After ultrasonic cleaning of raw CT and NCO-B-CT, the obtained bacterial dispersion was also stained using a LIVE/DEAD® BacLight™ Bacterial Viability Kit (Molecular Probes, Eugene, OR) (Lin et al. 2018; Sun et al. 2016). Briefly, 0.75 μL of 3.34 mM SYTO9 stain and 0.75 μL of 30 mM PI stain were added to 0.5 mL of the bacterial suspension and then incubated in darkness for 15 min followed by washing in saline solution and centrifugation. Afterward, the resuspended stained bacteria were spotted (10 μL) on a microscopic slide and visualized under a fluorescence microscope.

2.6. Antifungal adhesion experiment

In order to evaluate the antifungal adhesion activity of NCO-B-CT, an "invasion experiment" (Shi et al. 2015; Xie et al. 2020) was carried out by employing *A. niger*. The concentration of fungal spore suspension was adjusted to 10^8 spores mL^{-1} for later use. NCO-B-CT and the control raw CT were cut into 15.0 ± 0.1 mm diameter sized circular samples, and they were fixed onto the malt extract agar medium after UV light sterilization. Then, 10 μL of fungal suspension was dropped in the center of the plate, equidistant to the test samples. The plate was placed in a mold incubator and thermostatic cultured at 30 °C. The fungi were allowed to grow and expand from the medium center to the sample surface. After 30 d incubation, fungal growth phenomena at different periods were observed and recorded with a camera. Antifungal adhesion capability was quantified by the measurement of the fungal colonized areas. For this test, each experiment was repeated for three times.

SEM (S-4700 Hitachi) was used to observe the morphology of fungal cells on raw CT and NCO-B-CT surface. After 30 d incubation, samples mentioned above were immobilized with 2.5% glutaraldehyde for 2 h at 4 °C. Then, fungal cells were dehydrated by 50, 60, 70, 80, 90, and 100%

196 ethanol for 20 min, respectively. Finally, the samples were vacuum-dried for 12 h prior to the SEM
197 observation.

198 **2.7. Safety assays**

199 **2.7.1. Zone of inhibition (ZOI) determination of the treated fabrics.**

200 ZOI determination is a method for detecting the dissolution/nondissolution types of antibacterial
201 materials (Lin et al. 2018). The ZOI of raw CT and NCO-B-CT against *E. coli* and MRSA were
202 determined by diffusion method on an agar plate according to the GB/T 31713-2015 standard method.

203 **2.7.2. Skin sensitization evaluation**

204 According to the modified ISO 10993.10-2010 standard method (Chen et al. 2011; Xu et al. 2019a;
205 Zhang et al. 2018), skin sensitization of NCO-B-CT was evaluated. Three healthy male albino rabbits
206 (2.0–2.5 kg) were purchased from the Beijing Vital River Experimental Animal Technology Co., Ltd.,
207 and they were treated and cared for in accordance with the National Institutes of Health Guide for the
208 Care and Use of Laboratory Animals (NIH Publications No. 8023, revised 1978). In order to facilitate
209 material's contact with the skin, their backs were shaved to form a 10 × 10 cm^2 exposed area. As
210 illustrated in Fig. S1(Supporting Information), two NCO-B-CT and two raw CT control (2.5 × 2.5 cm^2)
211 were directly applied to the exposed area of the skin. After 6 h, the dressings were removed, the
212 positions of the samples were marked with pen. The skin sensitization appearances of each position
213 were recorded at 0, 1, 24, 48 and 72 h after material contact. According to the ISO 10993.10-2010
214 standard (Table S1), all erythema scores and edema scores at 24, 48 and 72 h were recorded. Calculated
215 the primary irritation score for each animal through dividing the sum of all scores by 6 (two test sites,
216 three time-points), and obtained the primary irritation index by taking the average scores of the three
217 rabbits. Table S2 shows the primary irritation index categories of the rabbits according to the ISO

10993.10-2010 standard. In addition, the skin tissue samples after contacting with raw CT and NCO-B-CT were sliced and stained with hematoxylin and eosin (H&E) for histopathological evaluation.

2.7.3. Cytotoxicity evaluation

The cytotoxicity of NCO-B-CT was evaluated by MTT test based on the ISO 10993.5-2009 standard method (Cao et al. 2020; Xin et al. 2020). Briefly, L929 mouse fibroblast cells were cultured in RPMI 1640 medium, supplemented with 10% FBS, 100 units mL^{-1} penicillin and 100 μg mL^{-1} streptomycin, at 37 ºC in a humidified atmosphere containing 95% air and 5% CO_2. After sterilizing with UV light, the raw CT and NCO-B-CT (0.1 g/mL) were immersed in RPMI 1640 medium (2 mL) at 37 ºC for 24 h. Then, the extraction solution was obtained and incubated with L929 cells for 48 h. Thereafter, the cells were subjected to an MTT assay and absorbance values were measured at 570 nm using a microplate reader. The cell relative growth rate (RGR) was calculated based on the following formula:

$$RGR\ (\%) = Abs_{570\ sample} / Abs_{570\ control} \times 100 \quad (3)$$

where $Abs_{570sample}$ and $Abs_{570control}$ are the absorbance of the sample and the reference at 570 nm, respectively.

2.8. Washing durability and usability test

According to the FZ/T 73023-2006 standard method, antimicrobial durability of NCO-B-CT was evaluated by an accelerated washing test (Xu et al. 2019a; Yu et al. 2016). Antibacterial adhesion rate of *E. coli* and MRSA, fungal colonized area of *A. niger* after 30 days of incubation and WCA of the treated NCO-B-CT were measured after 10, 20, 30, 40, and 50 times of repetitive washing cycles. Each experiment was carried out three times and the data were presented as mean ± SD. The chemical structure of NCO-B-CT before and after 50 times repeated washing was also determined by ATR-FTIR and XPS spectroscopy analyses.

According to the GB/T 3923.1-1997 standard (Xu et al. 2019a; Xu et al. 2021), tensile strength and elongation at break of raw CT and NCO-B-CT (the warp and weft directions) were measured by a testing machine (MTS Systems Co., Ltd., Shanghai, China). Each sample was tested five times and the mean values were recorded for further analysis.

2.9. Statistical analysis

Statistical analysis of all test data was performed using SPSS 16.0 software. All statistical data are expressed as mean ± standard deviation. After confirming normal distribution, two-tailed Student's *t*-tests were conducted to evaluate the differences between groups; *p*-values < 0.05 was considered significant.

3. Results and discussion

3.1. Characterization of NCO-B

Fig. S2a presents the FT-IR spectrum of NCO-B, the band at 2265 cm^{-1} is attributed to the characteristic stretching peak of NCO group. The −OH absorption peak of borneol at 3324 cm^{-1} was disappeared; Moreover, the bands at 3380 cm^{-1} and 1557 cm^{-1} ascribed to stretching vibration and deformation vibration of N−H group and the obvious new absorption peak at 1684 cm^{-1} ascribed to the stretching vibration of C=O in urethane group were found. These changes in the FT-IR spectra demonstrated the successful synthesis of NCO-B.

Furthermore, the ^{1}H-NMR spectrum (Fig. S2b) also shows the exact structure of NCO-B. The proton chemical shift of the borneol methyne group attached to the urethane group was clearly observed at δ 4.79 ppm. Other peaks of the cage structure of borneol were also found at δ 0.72–0.98, δ 1.15–1.80, δ

261 2.32 and δ 2.96 ppm. Additionally, the chemical shift for the methyne proton of IPDI appeared at δ 4.52
262 ppm. The chemical shift of methylene attached to the –NCO group appeared at δ 3.76 ppm. Multiple
263 peaks at δ 0.98–2.19 ppm can be attributed to other protons of IPDI. The results of ^{1}H NMR proved
264 that NCO-B was synthesized successfully.

265 **3.2. Characterization of NCO-B-CT**

266 As shown in Scheme 1, the NCO group of NCO-B reacted with the OH group on the CT surface to
267 generate the urethane group of NCO-B-CT. Because of the single layer modification with NCO-B
268 molecules, the NCO-B-CT maintained the same appearance of the raw CT, where the whiteness of the
269 fabrics remained basically unchanged (raw CT: 85.65; NCO-B-CT: 85.42). The enlarged SEM image
270 (Fig. 1a) also did not show any differences in the fiber surface. This modification was then evaluated
271 through WCA analysis (Fig. 1a). The hydrophobicity of NCO-B-CT was obviously increased (WCA:
272 135°) compared with that of raw CT (WCA: 32°), indicating the modification of hydrophobic NCO-B
273 molecules on the CT surface. EDS elemental mapping was performed to detect the surface elemental
274 distributions of raw CT and NCO-B-CT (Fig. 1a). Compared with raw CT, which had only C and O
275 signals on the surface, new signal of N was detected on the NCO-B-CT surface. The uniform
276 distribution of N also proved the homogeneous grafting of NCO-B on NCO-B-CT. Additionally, the
277 C/O ratio of NCO-B-CT (C: 62.25 at%, O: 35.31 at%) was increased to 1.76 as compared with the ratio
278 of 1.32 for raw CT (C: 56.98 at%, O: 43.02 at%) due to the presence of borneol C_{10} groups. The degree
279 of grafting (DG) of NCO-B-CT was 17.2%.

280 In addition, the surface chemical states studied by XPS are shown in Fig. 1b. Compared with raw
281 CT, which only had C1s (286.2 eV) and O1s (532.7 eV) characteristic signals, a new signal of N1s

(399.4 eV) was detected for NCO-B-CT, which was assigned to a −OCONH− bond (Fig. S3) (Wei et al. 2010). The C/O ratio of NCO-B-CT was also increased compared with that of raw CT. To further confirm the details, the compositions of C and O elements were analyzed. As shown in Fig. S4a, the C1s spectrum of raw CT included three deconvoluted peaks located at 283.4 eV, 284.8 eV and 286.3 eV, corresponding to the carbon atoms in C−C/C−H, C−O and O−C−O, respectively. For NCO-B-CT, the C1s region presented a new peak attributed to (C=O)−O band (288.5 eV) of NCO-B (Fig. S4b). Fig. S4a' and b′ show the O1s spectra of raw CT and NCO-B-CT. The peak shift from 531.3 eV (O−H and O−C) to 531.7 eV (O−H, O−C and O=C−O) also proved the successful modification of NCO-B-CT.

To further determine the characteristic functional groups, Fig. 1c presents the ATR-FTIR spectra of raw CT and NCO-B-CT. The raw CT was characterized with O−H stretching vibration (3070–3570 cm^{-1}), C−H stretching vibration (2805–3000 cm^{-1}) and C−O stretching vibration (1029 cm^{-1}) due to the cellulose glucose unit (Shi et al. 2015). For NCO-B-CT spectra, two new peaks at 1563 cm^{-1} and 1643 cm^{-1} were assigned to N−H deformation vibration and C=O stretching vibration, respectively, which can be observed in the FTIR spectra of NCO-B. The peaks at 3344 cm^{-1} and 2926 cm^{-1} were assigned to stretching vibration of N−H and $-CH_3$. Meanwhile, the band at 2265 cm^{-1} (the stretching vibration of NCO group) was disappeared at the ATR-FTIR spectrum of NCO-B-CT. These results supported the successful conjugation between NCO-B and raw CT.

3.3. Antibacterial adhesion capability

The antibacterial adhesion activities of NCO-B-CT were quantitatively assessed by viable cell count method against *E. coli* and MRSA. Fig. 2a presents the bacterial adhesion of both type of bacteria on

NCO-B-CT is obviously reduced as compared with that on raw CT. The number of bacteria adhered to the two samples was quantified in Fig. 2b. The bacterial adhesion number of both type of bacteria on NCO-B-CT was significantly less than that on raw CT ($p < 0.001$). The $\log_{10}$ reduction in bacterial adhesion count of NCO-B-CT is shown in Fig. 2c. NCO-B-CT resulted in a 1.66 $\log_{10}$ and 1.72 $\log_{10}$ (CFU mL^{-1}) reduction in bacterial adhesion count of *E. coli* and MRSA, respectively. As compared with raw CT, the antibacterial adhesion rates of NCO-B-CT against *E. coli* and MRSA were 97.6% and 98.1%, respectively. The results indicated that NCO-B-CT had an excellent antibacterial adhesion capability against both common bacteria (*E. coli*) and even drug-resistant superbugs (MRSA).

To further confirm the antibacterial mechanism of NCO-B-CT, the morphology of bacterial adhesion on raw CT and NCO-B-CT was intuitively observed by SEM, and bacteria adhered to the two samples were also investigated through LIVE/DEAD® BacLight™ fluorescent assays. As shown in Fig. 2d, bacteria can easily adhere to the surface of raw CT. Interestingly, almost no bacteria can be found on the surface of NCO-B-CT. In addition, the number of bacteria (green fluorescence of SYTO9 staining) adhered to the surface of NCO-B-CT was significantly reduced as compared with that on raw CT; moreover, no dead bacteria (red fluorescence of PI staining) were found on the NCO-B-CT surface (Fig. 2e). These results provide strong evidence that NCO-B-CT presents effective resistance to bacteria adhesion instead of killing bacteria, which is consistent with the stereochemical antimicrobial adhesion strategy (Xie et al. 2020).

3.4. Antifungal adhesion properties

In this study, *A. niger* was used as a test strain to evaluate the antifungal adhesion properties of NCO-B-CT through an “invasion experiment”. Fig. 3a presents the experimental model where the

control raw CT and NCO-B-CT were closely adhered on malt extract medium containing 10 μL of *A. niger* suspension added to the center of the plate.

As shown in Fig. 3b, fungi generally grew and expanded from the center to the border. After 1 days of incubation, *A. niger* spread to the edge of both raw CT and NCO-B-CT disks. After 4, 8 and 15 days of incubation, the fungal colonized areas of the control raw CT were 80.01, 99.11 and 100%, respectively (Fig. 3c). That is, the raw CT was very susceptible to contamination. In contrast, NCO-B-CT exhibited a clear surface and produced an obvious edge of fungal growth inhibition even after 30 days of incubation (Fig. 3b); and the fungal colonized areas was only 4.20% (Fig. 3c). SEM measurements were also used to detect microphenomena on the surface of the samples. Fig. 3d showed the morphologies of fungal cells adhered on the above-mentioned samples after 30 days of incubation. Numerous sporangia and hypha were found on the surface of raw CT. By contrast, no hypha and no spores were found on NCO-B-CT surface, only the modified cotton fibers could be observed. In other words, NCO-B-CT can effectively control the adhesion and growth of *A. niger* as compared with raw CT. The results demonstrated the excellent antifungal adhesion performance of NCO-B-CT.

3.5. Safety evaluation

According to the safety evaluation standards of antimicrobial textiles, solubility of the antibacterial agent, skin sensitization, and cytotoxicity were evaluated for NCO-B-CT.

3.5.1. ZOI tests

As shown in Fig. S5, the ZOIs of NCO-B-CT against *E. coli* and MRSA were both zero. That is, NCO-B-CT is a non-releasing antibacterial CT, thus ensuring the safety of its usage.

3.5.2. Skin sensitization test

To further ensure the safety of NCO-B-CT, skin sensitization test was performed on healthy albino

rabbits. As shown in Fig. 4a, after 0, 1, 24, 48, and 72 h of observation, neither erythema nor edema was found on the rabbit back skin after contacting with the NCO-B-CT sample and the raw CT control. For each animal, the skin erythema and edema scores at 24, 48, and 72 h after removing the sample and the control were all 0 (Table S3). Therefore, the primary irritation index of NCO-B-CT and raw CT were both 0 (Table S4). According to the standard (Table S2), the obtained index represents a negligible irritation, confirming that NCO-B-CT had no skin irritation or sensitization. Additionally, after contacting with CT and NCO-B-CT, the skin H&E staining results revealed no obvious histopathological abnormalities (Fig. 4b). These phenomena also indicated that the structure of NCO-B-CT was stable, and no release of NCO-B small molecules occurred during the usage.

3.5.3. Cytotoxicity evaluation

MTT assay was performed to further confirm the NCO-B-CT biocompatibility. Fig. 4c presents the RGR results of L929 cells for all test samples. After 48 h of incubating, the cell RGR after contact with raw CT and NCO-B-CT was 96.98 ± 7.58% and 96.34 ± 6.98%, respectively, which had no statistical differences ($p > 0.05$). The cytotoxicity grades of raw CT and NCO-B-CT were both 1 based on the classification standard GB/T 14233.2-2005 of cytotoxic response. Overall, NCO-B-CT was non-cytotoxic and had good biocompatibility, which can ensure its safe use.

3.6. Durability and usability

The antimicrobial adhesion durability of NCO-B-CT was evaluated from the perspective of its real-world applicability. As shown in Fig. 5a and b, after 50 times repetitive washing cycles, the antibacterial adhesion rates of NCO-B-CT against *E. coli* and MRSA were still above 92% and 95%, respectively. The fungus-covered area on NCO-B-CT after 30 days of incubation was only 8.61% which was considerably lower than that on raw CT (100%), and its resistance grade remained at level 1

368 based on the GB/T24346-2009 standard.

369 The antimicrobial adhesion durability is attributed to its structural stability. The hydrophobic
370 property of NCO-B-CT was maintained with a WCA of 132° after 50 repetitive washing cycles (Fig.
371 5c). The structure of NCO-B-CT after 50 laundering cycles was re-evaluated by ATR-FTIR and XPS.
372 As shown in Fig. 5d and S6, before and after 50 successive washing cycles, XPS and ATR-FTIR
373 spectra of the NCO-B-CT were similar, which supported that there was no change in the molecular
374 structures. The characteristic absorption peaks at 1563 cm^{-1} and 1643 cm^{-1} which were assigned to
375 N−H deformation vibration and C=O stretching vibration, and the peaks at 3344 cm^{-1} and 2926 cm^{-1}
376 which were assigned to stretching vibration of N−H and $-CH_3$ were remained. The N1s signal of the
377 sample which was assigned to the −OCONH− bond also showed no weakness. Thus, this finishing
378 method was strong enough to survive 50 times washing cycles.

379 The mechanical properties are also important for CT application. After testing, the mechanical
380 properties of NCO-B-CT were also improved. As shown in Fig. 6, the breaking strength increased from
381 310 ± 26 N to 354 ± 38 N in the weft direction, and from 486 ± 30 N to 521 ± 24 N in the warp
382 direction. Meanwhile, the breaking elongation was improved from 10.36 ± 1.24% to 13.18 ± 1.54% in
383 the weft direction, and from 23.42 ± 1.58% to 27.69 ± 1.89% in the warp direction. These results
384 indicated that the modifying of NCO-B enhanced the mechanical properties of the cotton fibers.
385 Overall, the NCO-B-CT material exhibited good usability and application potential.

386

387 **4. Conclusion**

388 In this study, an agile one-step finishing method to prepare antimicrobial CT using NCO-B
389 chemically bonded onto the surface of CT has been developed. After finishing, NCO-B-CT exhibited

broad-spectrum and remarkable antimicrobial adhesion properties against both bacteria and fungi. It also presented an anti-superbug adhesion effect against MRSA, where the anti-adhesion rate reached more than 98%. NCO-B-CT is a novel non-leaching antimicrobial material based on stereochemical antimicrobial strategy which causes no skin sensitization and has good biocompatibility. Furthermore, NCO-B-CT displayed durable washing fastness by bearing 50 times laundering cycles, and the mechanical properties of CT were improved greatly through NCO-B antimicrobial finishing. Thus, this NCO-B-CT material would be of great significance in control the spread of unwanted microorganisms, and have potential applications in many fields, such as multifunctional textiles, medical and hygiene.

Acknowledgments

The authors thank the financial support of the Technological Innovation Service Capacity Building-Basic Scientific Research Expenses under Grant (QNJJ2021-15).

Conflict of interest

We declare that we have no competing financial interests or personal relationships that could have appeared to influence the work reported in this paper.

411 **References**

412 Bains D, Singh G, Kaur N, Singh N (2019) Development of biological self-cleaning wound-dressing
413 gauze for the treatment of bacterial infection. ACS Sustainable Chemistry & Engineering 7:969–
414 978

415 Bouslimani A, Porto C, Rath CM, Wang MX, Guo YR, Gonzalez A, Berg-Lyon D, Ackermann G,
416 Christensen GJM, Nakatsuji T, Zhang LJ, Borkowski AW, Meehan MJ, Dorrestein K, Gallo RL,
417 Bandeira N, Knight R, Alexandrov T, Dorrestein PC (2015) Molecular cartography of the human
418 skin surface in 3D. Proceedings of the National Academy of Sciences 112:E2120–E2129

419 Brown ED, Wright GD (2016) Antibacterial drug discovery in the resistance era. Nature 529:336–343

420 Cai Q, Yang S, Zhang C, Li Z, Li X, Shen Z, Zhu W (2018) Facile and versatile modification of cotton
421 fibers for persistent antibacterial activity and enhanced hygroscopicity. ACS Applied Materials &
422 Interfaces 10:38506–38516

423 Cao Y, Gu J, Wang S, Zhang Z, Yu H, Li J, Chen S (2020) Guanidine-functionalized cotton fabrics for
424 achieving permanent antibacterial activity without compromising their physicochemical properties
425 and cytocompatibility. Cellulose 27:6027–6036

426 Chen S, Chen S, Jiang S, Xiong M, Luo J, Tang J, Ge Z (2011) Environmentally friendly antibacterial
427 cotton textiles finished with siloxane sulfopropylbetaine. ACS Applied Materials & Interfaces
428 4:1154–1162

429 Chen S, Yuan L, Li Q, Li J, Zhu X, Jiang Y, Sha O, Yang X, Xin JH, Wang J, Stadler FJ Huang P
430 (2016) Durable antibacterial and nonfouling cotton textiles with enhanced comfort via zwitterionic
431 sulfopropylbetaine coating. Small 12:3516–3521

Duan P, Xu Q, Zhang X, Chen J, Zheng W, Li L, Yang J, Fu F, Diao H, Liu X (2020) Naturally occurring betaine grafted on cotton fabric for achieving antibacterial and anti-protein adsorption functions. Cellulose 27:6603–6615

El-Naggar ME, Khattab TA, Abdelrahman MS, Aldalbahi A, Hatshan MR (2021) Development of antimicrobial, UV blocked and photocatalytic self-cleanable cotton fibers decorated with silver nanoparticles using silver carbamate and plasma activation. Cellulose 28: 1105–1121

Errokh A, Cheikhrouhou W, Ferraria AM, Botelho do Rego AM, Bouf S (2021) Cotton decorated with Cu_2O-Ag and Cu_2O-Ag-AgBr NPs via an in-situ sacrificial template approach and their antibacterial efficiency. Colloids and Surfaces B: Biointerfaces 200:111600

Fijan S, Turk SS (2012) Hospital textiles, are they a possible vehicle for healthcare-associated infections? International Journal of Environmental Research and Public Health 9:3330–3343

Fujimori A, Yamato R, Kikkawa T, Tatewaki Y (2015) Morphological transition of a conductive molecular organization with non-covalent from nanonetwork to nanofiber. Journal of Colloid and Interface Science 448:180–188

Gao D, Li Y, Lyu B, Jin D, Ma J (2020) Silicone quaternary ammonium salt based nanocomposite: a long-acting antibacterial cotton fabric finishing agent with good softness and air permeability. Cellulose 27:1055–1069

Gao D, Hou Y, Lyu B, Ma J, Li Y, Li Y (2021a) Antibacterial cotton with endurance and skin affinity treated by P(DMDAAC-AGE-Si)/(ZnO@CQDs). Cellulose 28: 593–606

Gao D, Li X, Li Y, Lyu B, Ren J, Ma J (2021b) Long-acting antibacterial activity on the cotton fabric. Cellulose 28:1221–1240

453 Gu J, Yuan L, Zhang Z, Yang X, Luo J, Gui Z, Chen S (2018) Non-leaching bactericidal cotton fabrics
454 with well-preserved physical properties, no skin irritation and no toxicity. Cellulose 25:5415–5426
455 Hoefer D, Hammer TR (2011) Antimicrobial active clothes display no adverse effects on the ecological
456 balance of the healthy human skin microflora. ISRN Dermatology 2:369603
457 Irfan M, Polonskyi O, Hinz A, Mollea C, Bosco F, Strunskus T, Balagna C, Perero S, Faupel F,
458 Ferraris M (2019) Antibacterial, highly hydrophobic and semi transparent
459 Ag/plasma polymer nanocomposite coating on cotton fabric obtained by plasma based co-
460 deposition. Cellulose 26:8877–8894
461 Jafari R, Amirshahi SH (2007) A comparison of the cie and uchida whiteness formulae as predictor of
462 average visual whiteness evaluation of textiles. Textile Research Journal 77:756–763
463 Karimi L, Yazdanshenas ME, Khajavi R, Rashidi A, Mirjalili ML (2014) Using graphene/TiO_2
464 nanocomposite as a new route for preparation of electroconductive, self-cleaning, antibacterial and
465 antifungal cotton fabric without toxicity. Cellulose 21:3813–3827
466 Li G, Zhao H, Hong J, Quan K, Yuan Q, Wang X (2017) Antifungal graphene oxide-borneol composite.
467 Colloids and Surfaces B: Biointerfaces 160:220–227
468 Li X, Xie Z, Li G, Tao L, Wei Y, Wang X (2021) Antifungal polymer containing menthoxy triazine.
469 ACS Applied Polymer Materials 3:3702–3707
470 Li Z, Chen J, Cao W, Wei D, Zheng A, Guan Y (2018) Permanent antimicrobial cotton fabrics
471 obtained by surface treatment with modified guanidine. Carbohydrate Polymers 180:192–199
472 Lin J, Chen XY, Chen CY, Hu JT, Zhou CL, Cai XF, Wang W, Zheng C, Zhang PP, Cheng J, Guo ZH,
473 Liu H (2018) Durably antibacterial and bacterially antiadhesive cotton fabrics coated by cationic
474 fluorinated polymers. ACS Applied Materials & Interfaces 10:6124−6136

475 Lin PA, Cheng CH, Hsieh KT, Lin JC (2014) Effect of alkyl chain length and fluorine content on the
476 surface characteristics and antibacterial activity of surfaces grafted with brushes containing
477 quaternized ammonium and fluoro-containing monomers. Colloids and Surfaces B: Biointerfaces
478 202:111674
479 Luo L, Li G, Luan D, Yuan Q, Wei Y, Wang X (2014) Antibacterial adhesion of borneol-based
480 polymer via surface chiral stereochemistry. ACS Applied Materials & Interfaces 6:19371–19377
481 Metcalf CJE, Lessler J (2017) Opportunities and challenges in modeling emerging infectious diseases.
482 Science 357:149–152
483 Munoz-Price LS, Arheart KL, Mills JP, Cleary T, DePascale D, Jimenez A, Fajardo-Aquino Y, Coro G,
484 Birnbach DJ, Lubarsky DA (2012) Associations between bacterial contamination of health care
485 workers' hands and contamination of white coats and scrubs. American Journal of Infection
486 Control 40:E245–E248
487 Pan NY, Liu Y, Ren XH, Huang TS (2018) Fabrication of cotton fabrics through in-situ reduction of
488 polymeric *N*-halamine modified graphene oxide with enhanced ultraviolet-blocking, self-cleaning,
489 and highly efficient, and monitorable antibacterial properties. Colloids and Surfaces A:
490 Physicochemical and Engineering Aspects 555:765–771
491 Qian H, Xu D, Du C, Zhang D, Li X, Huang L, Deng L, Tu Y, Mol JMC, Terryn HA (2017) Dual-
492 action smart coating with a self-healing superhydrophobic surface and anti-corrosion properties.
493 Journal of Materials Chemistry A 5:2355–2364
494 Qian Y, Qi F, Chen Q, Zhang Q, Qiao Z, Zhang S, Wei T, Yu Q, Yu S, Mao Z, Gao C, Ding Y, Cheng
495 Y, Jin C, Xie H, Liu R (2018) Surface modified with a host defense peptide-mimicking β-peptide

polymer kills bacteria on contact with high efficacy. ACS Applied Materials & Interfaces 10:15395–15400

Sadeghi-Kiakhani M, Tehrani-Bagha AR, Safapour S (2018) Enhanced anti-microbial, anti-creasing and dye absorption properties of cotton fabric treated with chitosan-cyanuric chloride hybrid. Cellulose 25:883–893

Shi B, Luan D, Wang S, Zhao L, Tao L, Yuan Q, Wang X (2015) Borneol-grafted cellulose for antifungal adhesion and fungal growth inhibition. RSC Advances 5:51947–51952

Simoncic B, Tomsic B (2010) Structures of novel antimicrobial agents for textiles - a review. Textile Research Journal 80:1721–1737

Song L, Sun L, Zhao J, Wang X, Yin J, Luan S, Ming W (2019) Synergistic superhydrophobic and photodynamic cotton textiles with remarkable antibacterial activities. ACS Applied Bio Materials 2:2756–2765

Su X, Chen W, Han Y, Wang D, Yao J (2021) In-situ synthesis of Cu_2O on cotton fibers with antibacterial properties and reusable photocatalytic degradation of dyes. Applied Surface Science 536:147945

Sun X, Qin Z, Luo L, Yuan Q, Guo X, Tao L, Wei Y, Wang X (2016) Antibacterial adhesion of poly (methyl methacrylate) modified by borneol acrylate. ACS Applied Materials & Interfaces 8:28522–28528

Thi VHT, Lee BK (2017) Development of multifunctional self-cleaning and UV blocking cotton fabric with modification of photoactive ZnO coating via microwave method. Journal of Photochemistry and Photobiology A: Chemistry 338:13–22

Velema WA, Van Der Berg JP, Hansen MJ, Szymanski W, Driessen AJ, Feringa BL (2013) Optical control of antibacterial activity. Nature Chemistry 5:924–928

Wang J, Chen Y, An J, Xu K, Chen T, Mueller-Buschbaum P, Zhong Q (2017a) Intelligent textiles with comfort regulation and inhibition of bacterial adhesion realized by cross-linking poly(n-isopropylacrylamide-co-ethylene glycol methacrylate) to cotton fabrics. ACS Applied Materials & Interfaces 9:13647–13656

Wang X, Gan H, Sun T, Su B, Fuchs H, Vestweber D, Butz S (2010) Stereochemistry triggered differential cell behaviours on chiral polymer surfaces. Soft Matter 6:3851–3855

Wang X, Gan H, Zhang M, Sun T (2012) Modulating cell behaviors on chiral polymer brush films with different hydrophobic side groups. Langmuir 28:2791–2798

Wang X, Jing S, Liu Y, Liu S, Tan Y (2017b) Diblock copolymer containing bioinspired borneol and dopamine moieties: synthesis and antibacterial coating applications. Polymer 116:314–323

Wang Y, Yin M, Li Z, Liu Y, Ren X, Huang TS (2018) Preparation of antimicrobial and hemostatic cotton with modified mesoporous particles for biomedical applications. Colloids and Surfaces B: Biointerfaces 165:199–206

Wei Q, Zhang F, Li J, Li B, Zhao C (2010) Oxidant-induced dopamine polymerization for multifunctional coatings. Polymer Chemistry 1:1430–1433

Wu M, Ma B, Pan T, Chen S, Sun J (2016) Silver-nanoparticle-colored cotton fabrics with tunable colors and durable antibacterial and self-healing superhydrophobic properties. Advanced Functional Materials 26:569–576

Xie Z, Li G, Wang X (2020) Chiral stereochemical strategy for antimicrobial adhesion. Racing for the Surface: Pathogenesis of Implant Infection and Advanced Antimicrobial Strategies, Springer, Switzerland, pp 431–456

Xin Y, Zhao H, Xu J, Xie Z, Li G, Gan Z, Wang X (2020) Borneol-modified chitosan: antimicrobial adhesion properties and application in skin flora protection. Carbohydrate Polymers 228:115378–115388

Xu J, Bai Y, Wan M, Liu Y, Tao L, Wang X (2018) Antifungal paper based on a polyborneolacrylate coating. Polymers 10:448–460

Xu J, Zhao H, Xie Z, Ruppel S, Zhou X, Chen S, Liang JF, Wang X (2019a) Stereochemical strategy advances microbially antiadhesive cotton textile in safeguarding skin flora. Advanced Healthcare Materials 8:1900232

Xu J, Xie Z, Du F, Wang X (2021) One-step anti-superbug finishing of cotton textiles with dopamine-menthol. Journal of Materials Science & Technology 69:79–88

Xu QB, Zheng WS, Duan PP, Chen JN, Zhang YY, Fu FY, Diao HY, Liu XD (2019b) One-pot fabrication of durable antibacterial cotton fabric coated with silver nanoparticles via carboxymethyl chitosan as a binder and stabilizer. Carbohydrate Polymers 204:42–49

Yang L, Zhan C, Huang X, Hong L, Fang L, Wang W, Su J (2020) Durable antibacterial cotton fabrics based on natural borneol-derived anti-MRSA agents. Advanced Healthcare Materials 92000186

Ye Z, Li S, Zhao S, Deng L, Zhang J, Dong A (2021) Textile coatings configured by double-nanoparticles to optimally couple superhydrophobic and antibacterial properties. Chemical Engineering Journal 420:127680

Yu M, Wang Z, Lv M, Hao R, Zhao R, Qi L, Liu S, Yu C, Zhang B, Fan C, Li J (2016) Antisuperbug cotton fabric with excellent laundering durability. ACS Applied Materials & Interfaces 8:19866–19871

Zhang Y, Xu Q, Fu F, Liu X (2016) Durable antimicrobial cotton textiles modified with inorganic nanoparticles. Cellulose 23:2791–2808

Zhang S, Yang X, Tang B, Yuan L, Wang K, Liu X, Zhu X, Li J, Ge Z, Chen S (2018) New insights into synergistic antimicrobial and antifouling cotton fabrics via dually finished with quaternary ammonium salt and zwitterionic sulfobetaine. Chemical Engineering Journal 336:123–132

Figure captions

Scheme 1 Schematic illustration of the one-step finishing of NCO-B-CT, "R" represents the group in the red-dotted lines box

Fig. 1 Characterization of NCO-B-CT and the control group of raw CT. **a** SEM images and the corresponding EDS mapping of C (red), O (green), and N (pink) elements. The scale bar is 200 μm. The inset shows the corresponding WCA measurement. **b** XPS spectra. **c** ATR-FTIR spectra

Fig. 2 Antibacterial adhesion capability of NCO-B-CT. **a** Colony images of bacteria adhered to NCO-B-CT and the control raw CT. **b** Statistical amounts of bacteria adhered to NCO-B-CT and the control. Error bars indicate standard deviations (n = 3, *** $p < 0.001$). **c** Reduction in bacterial adhesion count of BDCT compared with raw CT. Data presented as mean ± SD, n=3. **d** SEM images of the adhered bacteria (*E. coli* and MRSA) on the control raw CT and treated NCO-B-CT. The scale bar is 10 μm. **e** LIVE/DEAD® BacLightTM fluorescence assay of bacteria adhered (*E. coli* and MRSA) to the control raw CT and treated NCO-B-CT. The scale bar is 50 μm

Fig. 3 Evaluation of antifungal adhesion properties. **a** Illustration of antifungal adhesion model. **b** Digital photos of the anti-adhesion effects of raw CT and NCO-B-CT by culturing *A. niger* in the center of the solid medium for the indicated days. **c** Fungal colonized area of *A. niger* on raw CT and NCO-B-CT after 0, 1, 4, 8, 15 and 30 days of incubation. Data presented as mean ± SD, n = 3. **d** SEM images of the adhered *A. niger* on raw CT and NCO-B-CT surfaces. Left are images at low magnifications; right are images at high magnifications

Fig. 4 Safety assays. **a** Skin irritation and sensitization test of NCO-B-CT and raw CT control according to the ISO 10993.10-2010 standard. The images display the backs of rabbits contacting the raw CT control (in the circles marked with black-dotted lines) and NCO-B-CT sample (in the circles

marked with red-dotted lines) at 0, 1, 24, 48, and 72 h. **b** The histopathological analysis of skin with H&E staining for skin contacted with raw CT control and NCO-B-CT at 72 h. **c** RGR of L929 cells for 48 h of incubation in conditioned media containing an extraction solution of raw CT and NCO-B-CT. Error bars indicate standard deviations (n = 3)

Fig. 5 Washing durability test of NCO-B-CT according to the FZ/T 73023-2006 standard. **a** Antibacterial adhesion rate of NCO-B-CT against *E. coli* and MRSA after 0, 10, 20, 30, 40 and 50 times of repetitive washing cycles. Data presented as mean ± SD, n = 3. **b** Fungal colonized area of *A. niger* after 30 days of incubation on raw CT and NCO-B-CT after 0, 10, 20, 30, 40 and 50 times of repetitive washing cycles. Data presented as mean ± SD, n = 3. **c** WCA of NCO-B-CT after 0, 10, 20, 30, 40 and 50 times of repetitive washing cycles. Data presented as mean ± SD, n = 3. **d** ATR-FTIR survey spectra of NCO-B-CT before and after 50 successive washing cycles

Fig. 6 Mechanical properties of NCO-B-CT. (**a**) Breaking strength and (**b**) breaking elongation of raw CT and NCO-B-CT. Error bars indicate standard deviations (n = 5)

Figures list

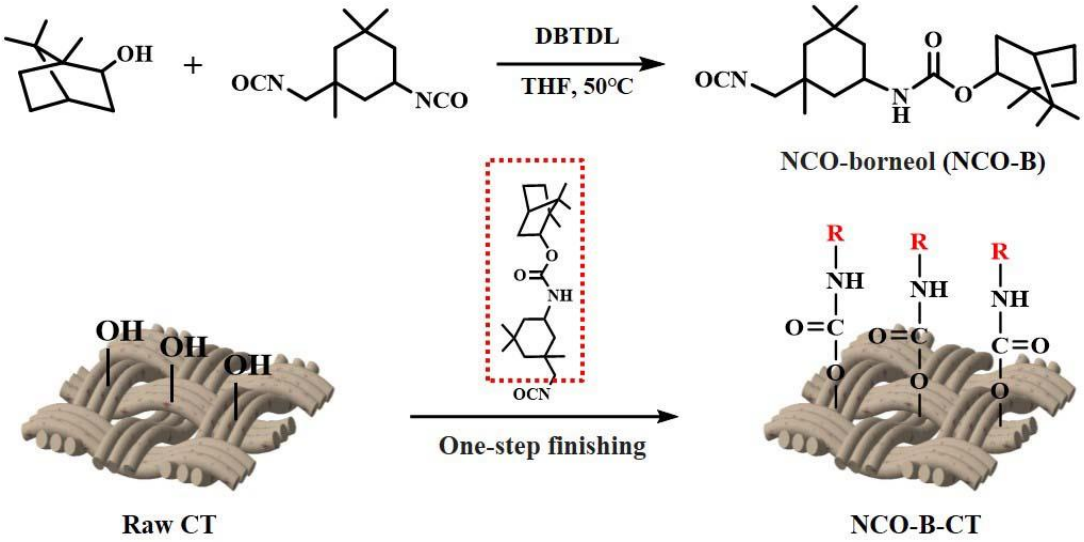

Scheme 1

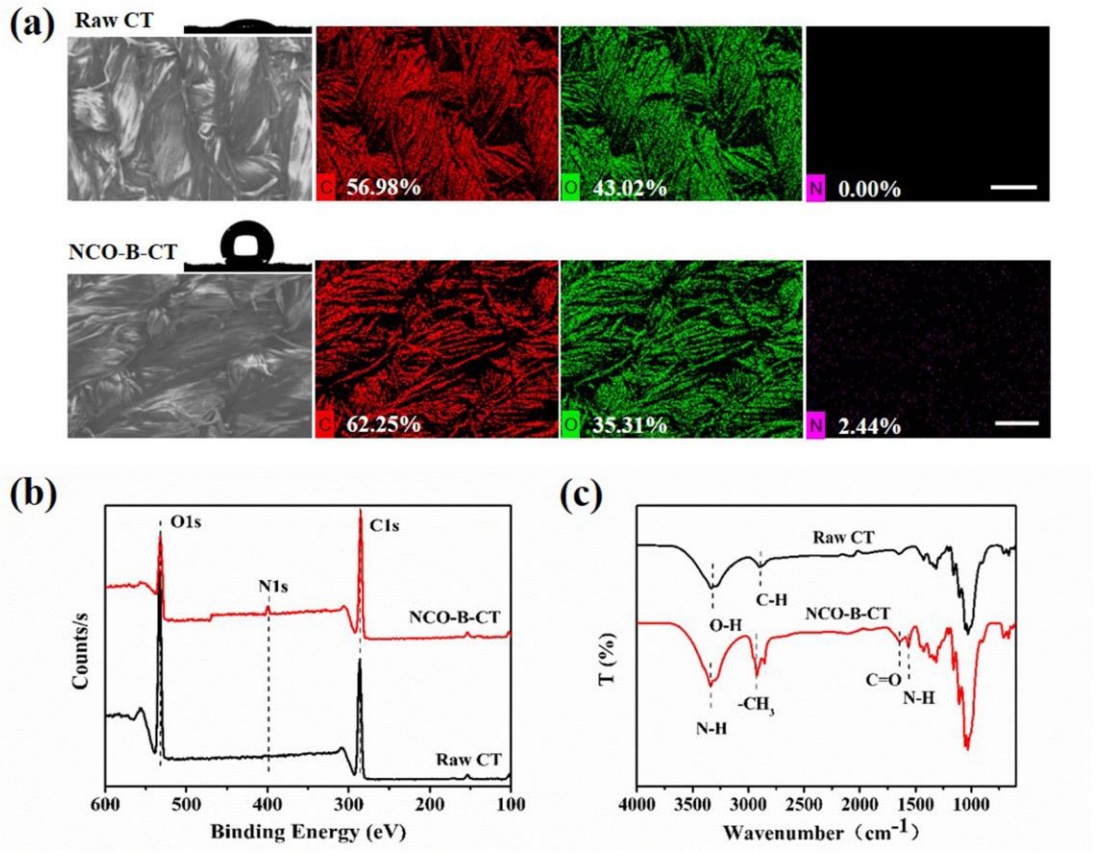
(a)
Raw CT
C 56.98%
O 43.02%
N 0.00%
NCO-B-CT
C 62.25%
O 35.31%
N 2.44%
(b)
O1s
C1s
N1s
NCO-B-CT
Raw CT
Counts/s
600 500 400 300 200 100
Binding Energy (eV)
(c)
Raw CT
C-H
O-H
NCO-B-CT
C=O
N-H
-CH3
N-H
T (%)
4000 3500 3000 2500 2000 1500 1000
Wavenumber (cm-1)

Fig. 1

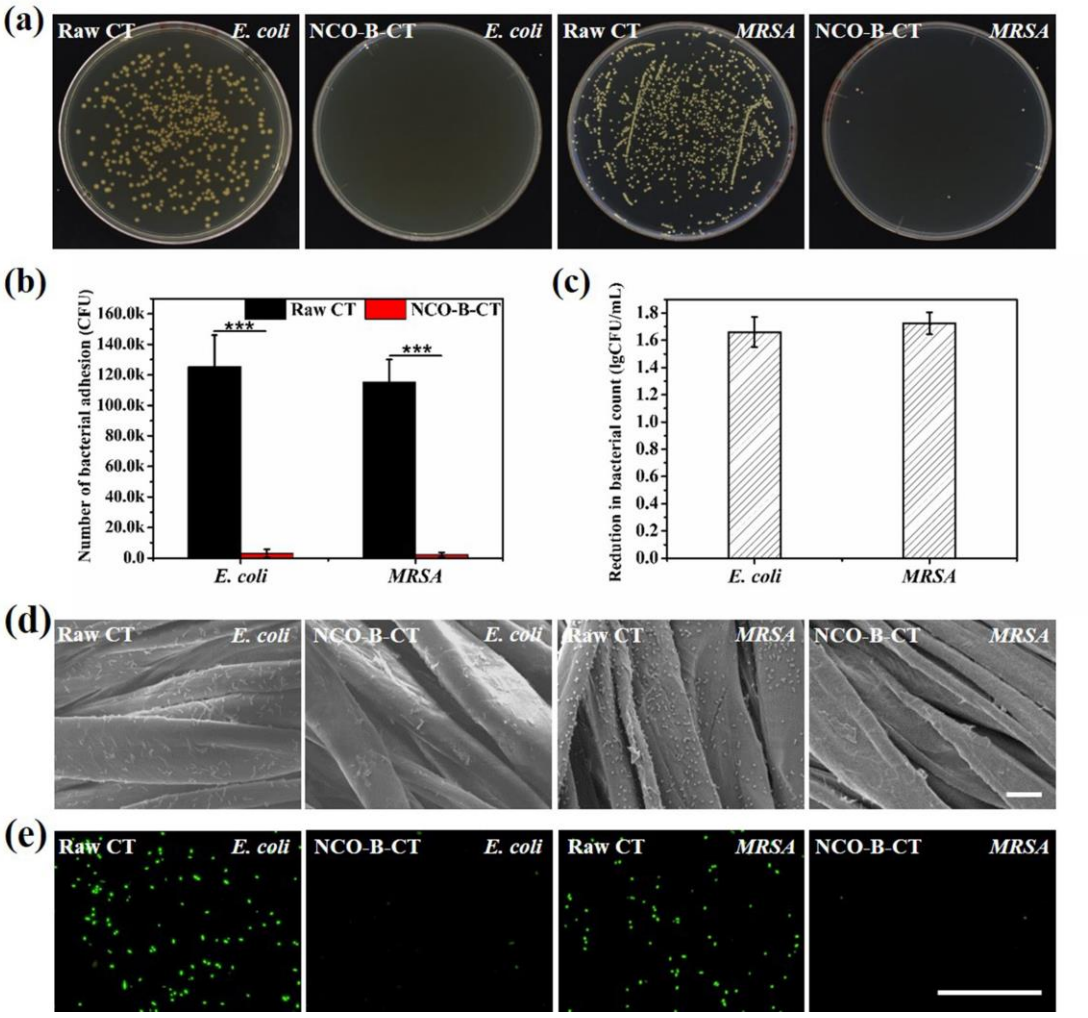
(a)
Raw CT
E. coli
NCO-B-CT
E. coli
Raw CT
MRSA
NCO-B-CT
MRSA
(b)
Number of bacterial adhesion (CFU)
160.0k
140.0k
120.0k
100.0k
80.0k
60.0k
40.0k
20.0k
0.0
Raw CT
NCO-B-CT
***
***
E. coli
MRSA
(c)
Redution in bacterial count (lgCFU/mL)
1.8
1.6
1.4
1.2
1.0
0.8
0.6
0.4
0.2
0.0
E. coli
MRSA
(d)
Raw CT
E. coli
NCO-B-CT
E. coli
Raw CT
MRSA
NCO-B-CT
MRSA
(e)
Raw CT
E. coli
NCO-B-CT
E. coli
Raw CT
MRSA
NCO-B-CT
MRSA

Fig. 2

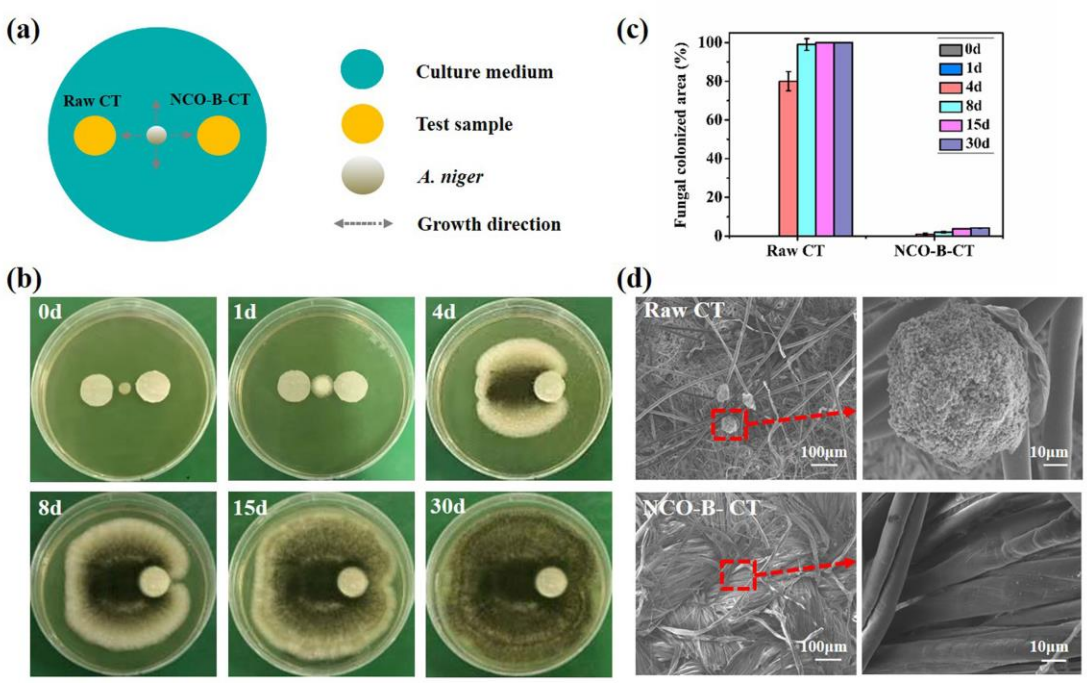
(a)
Raw CT
NCO-B-CT
Culture medium
Test sample
A. niger
Growth direction
(c)
Fungal colonized area (%)
0d
1d
4d
8d
15d
30d
Raw CT
NCO-B-CT
(b)
0d
1d
4d
8d
15d
30d
(d)
Raw CT
NCO-B- CT
100μm
10μm

Fig. 3

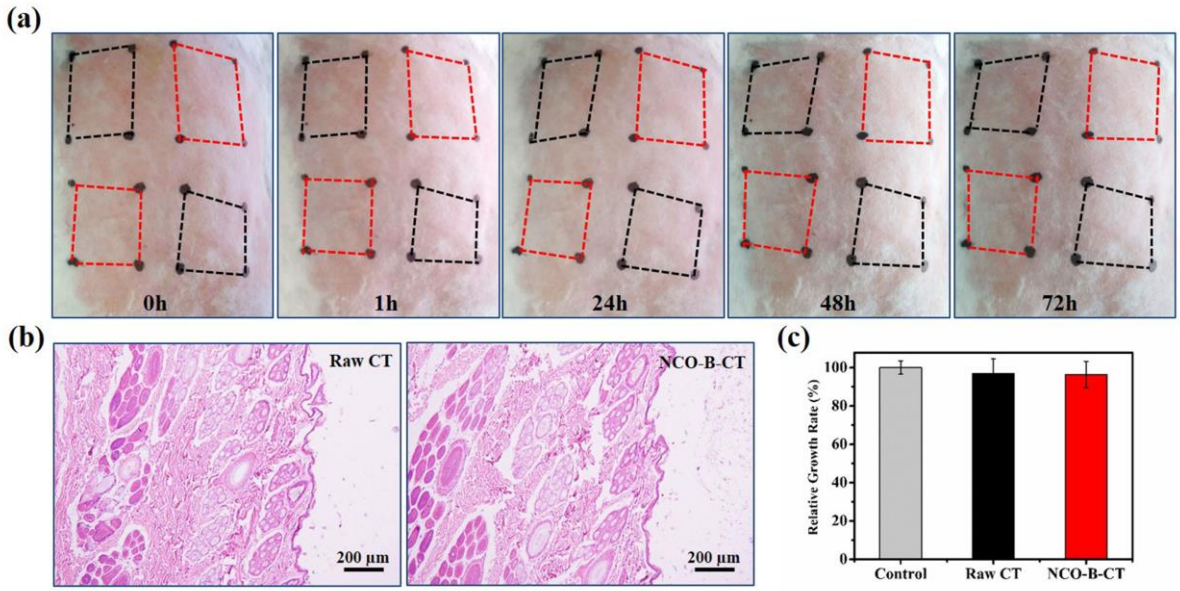

676

677 **Fig. 4**

678

679

680

681

682

683

684

685

686

687

688

689

690

691

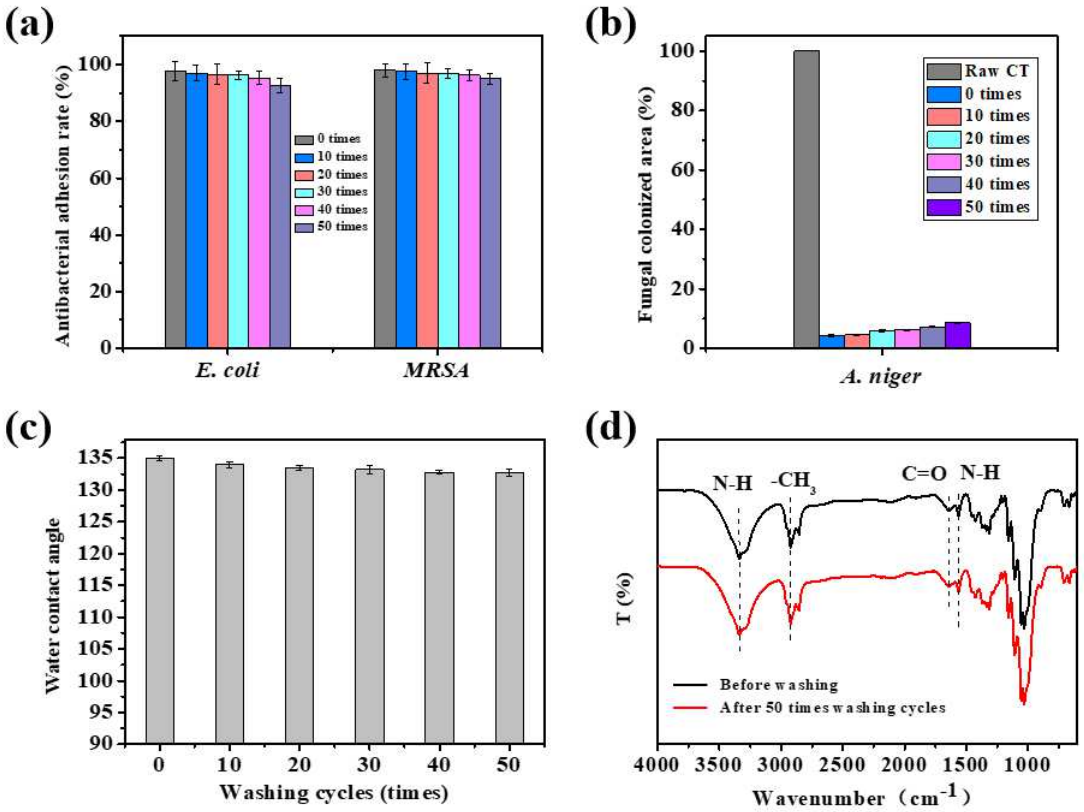

692

693 **Fig. 5**

694

695

696

697

698

699

700

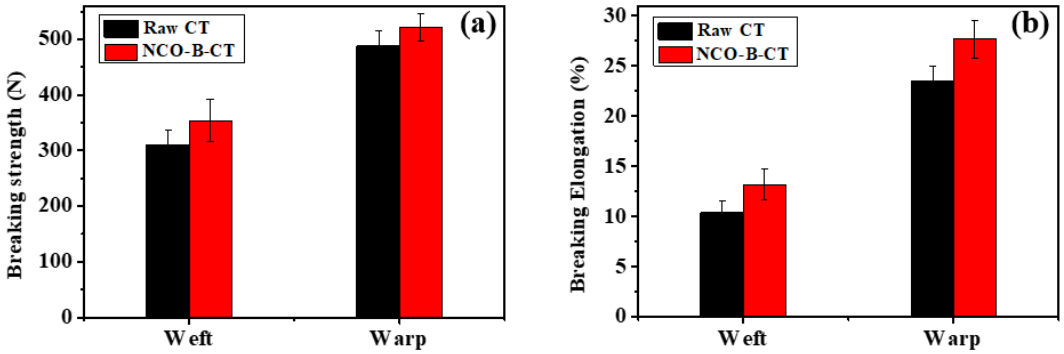
(a)
Raw CT
NCO-B-CT
Breaking strength (N)
0
100
200
300
400
500
Weft
Warp
(b)
Raw CT
NCO-B-CT
Breaking Elongation (%)
0
5
10
15
20
25
30
Weft
Warp

701

702 **Fig. 6**

Supplementary Files

This is a list of supplementary files associated with this preprint. Click to download.

- SupportingInformationNCOBCT.pdf